Disk heat transfer in a rotating cavity with an axial throughflow of cooling air

C. A. Long
Thermo-Fluid Mechanics Research Centre, School of Engineering, University of Sussex, Brighton, UK

A heated, rotating cavity with an axial throughflow of air is used as an experimental model for a pair of gas turbine, high-pressure compressor disks. Tests were carried out on a single rotating cavity comprising two disks of radius $b = 0.4845$m, bounded at the circumference by a carbon fiber shroud. Experiments were conducted with and without a heated shroud and for the range of parameters: $0.03 \leq \beta\Delta T \leq 0.3$; $2 \times 10^3 \leq Re_z \leq 16 \times 10^4$ and $2 \times 10^5 \leq Re_\phi \leq 5 \times 10^6$; for cavity gap ratios $G = 0.13$ and 0.36, and a constant value of inlet radius ratio of $a/b = 0.1$. Measurements were also made of the air temperature inside the cavity by three thermocouple probes. The heat transfer from the disks was measured using thermopile flux meters.

The measurements of cavity air temperature and cavity heat transfer were used to estimate the fraction of the central throughflow entering the cavity. This shows only a slight dependence on the gap ratio. For $Ro < 1$, approximately 50 percent is found to enter the cavity; for $Ro > 10$, this decreases to around 10 percent.

Two mechanisms appear to operate in influencing the heat transfer. Firstly, heating of the air inside the cavity destablizes it and convection occurs under the action of rotationally induced buoyancy forces. Secondly, the central throughflow encourages mixing with the cavity air, which can either affect the heat transfer directly (as, for example, at the inner radii of the disks) or indirectly through the action of vortex breakdown. For the smaller gap ratio cavity, rotational effects become increasingly important toward the outer radius across a wide range of Rossby numbers. For the wider gap ratio cavity, this is restricted to a narrower range of Ro. In the region $4 \leq Ro \leq 5$, the gap ratio plays a crucial role in affecting the disk heat transfer. At smaller values of Ro, where a significant fraction of the throughflow enters the cavity, the disk heat transfer rate does not appear to be affected by the gap ratio. At larger values, increasing the gap ratio also increases the heat transfer.

Keywords: gas turbine internal air systems; heat transfer; rotating cavity with axial throughflow; rotating flow; rotationally induced buoyancy

1. Introduction

In modern aircraft gas turbines, it is common practice to supply cooling air to the turbine disks and blades. As illustrated in Figure 1, this cooling air, usually obtained from successive stages of the intermediate-pressure compressor, flows axially between the bores of adjacent disks in the high-pressure compressor. Some of this axial throughflow enters the cavities formed between the disks and a parasitic temperature rise occurs as a result of the convective heat transfer from the disk surfaces and peripheral shroud. A knowledge of the heat transfer in these compressor cavities is important for two reasons. Firstly, the engine designer obviously needs to predict the temperature of the turbine cooling air. Secondly, the designer needs to know the temperature of the compressor disks to calculate the stress, radial growth and life.

A simplified version of this comprises a cylindrical cavity formed by two disks of outer radius b and a peripheral shroud of axial width s. The flow structure and heat transfer for the case when only the disks are heated was studied by Farthing et al. (1992a, 1992b). They found that rotationally induced buoyancy forces caused the flow to enter the cavity. The heat transfer from the disks was correlated and for $G = s/b = 0.13$, they found the local Nusselt numbers to depend on both the Reynolds number of the axial throughflow, Re_z, and a rotational Grashof number, Gr. One particularly significant finding was that the appropriate characteristic length for the Nusselt and Grashof numbers was the distance measured radially inward from the shroud—implying that a boundary layer flows in this direction. Another was the form of correlation, between the local Nusselt numbers on the disks and the Grashof number, having an exponent of 1/4—a value usually associated with laminar flow. In this previous work, the shroud was unheated. But in an engine, the shroud can (particularly under acceleration and steady-state conditions) be hotter than the disks and in addition to contributing to the total heat transfer in a cavity, this may also affect the heat transfer from the disks.

The work reported in this paper compares disk heat transfer measurements (with and without a heated shroud) for $G = 0.13$ to those for the case of $G = 0.36$. A review of relevant aspects of the flow structure and heat transfer in a cavity with an axial throughflow is given in Section 2. The experimental apparatus is briefly described in Section 3. Experiments were conducted

Address reprint requests to Dr. C. A. Long at the Thermo-Fluid Mechanics Research Centre, School of Engineering, University of Sussex, Brighton, BN1 9QT, Sussex, UK.

Received 2 February 1993; accepted 30 March 1994

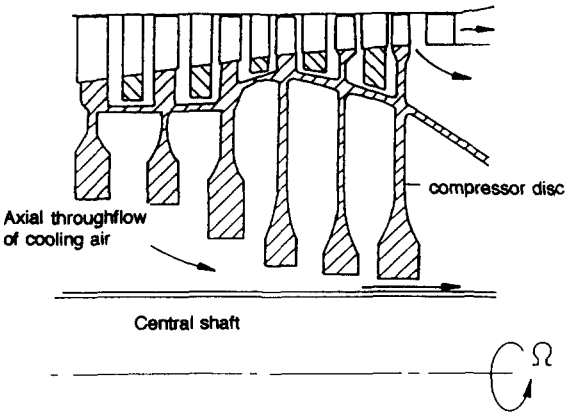

Figure 1 Simplified arrangement of a high-pressure compressor drum

to measure the temperature of the air inside the cavity itself and also the heat transfer from the disks; these are discussed in Sections 4 and 5, respectively. Finally, conclusions and some recommendations for the direction of future research are given in Section 6.

2. Background: flow structure and heat transfer in a rotating cavity with axial throughflow of cooling air

The current understanding of the flow structure in a heated rotating cavity with an axial throughflow of cooling air is described by Farthing et al. (1992b). A brief description of their work will be given here as it will aid the discussion given in this paper.

The essential features of the flow structure are illustrated in Figure 2. The rotational speed of the cavity is Ω and the bulk average velocity of the throughflow is *W*. When the disks are unheated, the flow structure is similar to that shown in Figure

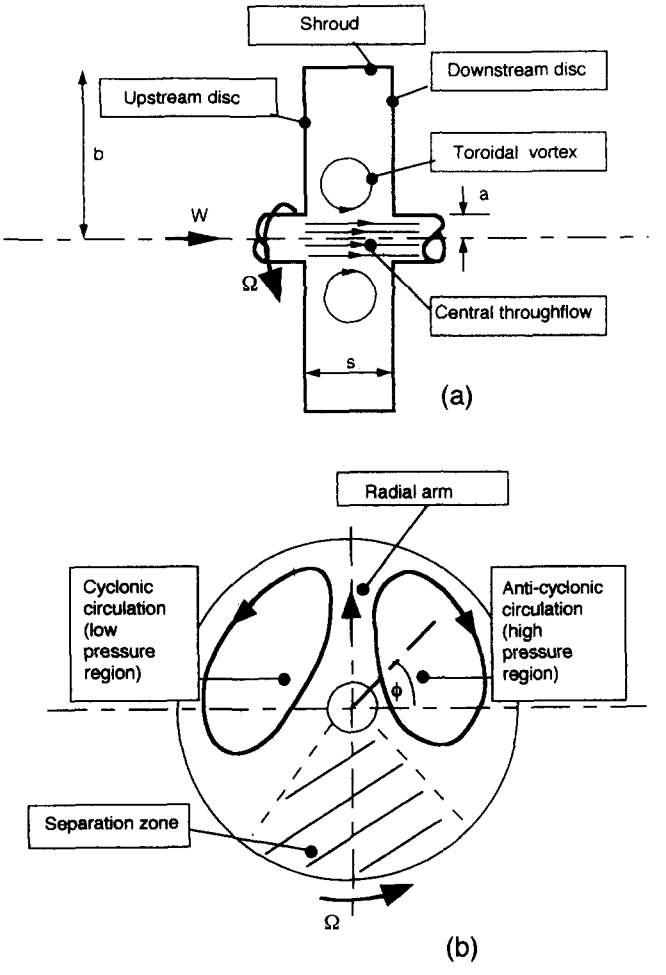

Figure 2 Schematic diagrams of flow structure in a rotating cavity with an axial throughflow: (a) isothermal flow, $T_s = T_i$(r-z plane); (b) heated flow, $T_s > T_i$(r-ϕ plane)

Notation

a, b	Inner and outer radius of cavity
C_o	Constant
C_p	Specific heat at constant pressure
G	Cavity gap ratio ($G = s/b$)
Gr	Rotational Grashof number ($\mathrm{Gr} = \Omega^2 r(b-r)^3 \beta \Delta T/\nu^2$)
k	Thermal conductivity
M	Fraction of throughflow to enter cavity
n	Constant
Nu	Nusselt number ($\mathrm{Nu} = qr/\Delta T k$)
Pr	Prandtl number ($\mathrm{Pr} = \mu Cp/k$)
q	Heat flux
r	Radial coordinate
Re_z	Axial Reynolds number ($\mathrm{Re}_z = 2aW/\nu$)
Re_ϕ	Rotational Reynolds number ($\mathrm{Re}_\phi = \Omega b^2/\nu$)
Re_ϕ^*	Local rotational Reynolds number ($\mathrm{Re}_\phi^* = \Omega r^2/\nu$)
Ro	Rossby number ($\mathrm{Ro} = W/\Omega a$)
s	Axial gap between the disks
t	Time
T	Temperature
W	Bulk average velocity of throughflow
x	Nondimensional radial coordinate ($x = r/b$)
z	Axial coordinate

Greek symbols

$\beta = 1/T$	Volume expansion coefficient
ΔT	Temperature difference
θ	Temperature ratio
ν	Kinematic viscosity
μ	Dynamic viscosity
ϕ	Tangential coordinate
ω	Circumferentially averaged rotational speed of the fluid in the cavity
Ω	Rotational speed of the disks

Subscripts, superscripts

av	Denotes a radially weighted average
cav	Pertains to conditions inside the cavity
i	Inlet value
max	Maximum value
s	Pertains to the disk surface
sh	Pertains to the shroud

2a. In this case, the central jet passing through the cavity (the throughflow) generates a toroidal vortex. In the absence of vortex breakdown, the flow is two-dimensional and there is virtually no penetration of the throughflow into the cavity itself.

When the disks are heated, there is a dramatic change in the flow structure, which becomes three-dimensional (3-D) and is driven by buoyancy effects that are themselves induced by rotation. The following description of the resulting flow is based on observations of the flow in a cavity with a surface temperature distribution that decreases with radius. It was found that this gave a clearly defined structure. For a surface temperature distribution that increases with radius, considerably more of the throughflow appears to penetrate the cavity and the features of the flow are less easily discernible. A schematic of the heated flow structure (given in the r-ϕ plane, as this best illustrates the relevant features) is shown in Figure 2b. In the region between the two disks, the heated flow structure comprises a radial arm, a pair of circulation regions and another region separating them. These elements of the flow structure rotate at an angular velocity ω, which varies with gap ratio, the Rossby number, Ro ($= W/\Omega a$) and thermal conditions, but typically $0.9 < \omega/\Omega < 1$. Fluid in the radial arm enters the cavity, bifurcates at the shroud and forms the two regions of circulation. The cyclonic region rotates in the same direction as the disks; the anticyclonic region rotates in the opposite direction. The regions of circulation do not merge, but are separated by another region into which fluid does not appear to enter and is referred to as the separation zone. Because the circulations rotate in opposite directions, they are at different pressures and, just as their meteorological equivalents, the cyclonic region has a lower pressure than the anticyclonic region. The physical consequence is that a circumferential variation of pressure provides a Coriolis force that is necessary for radial flow in the inviscid region between the two disks.

Farthing (1988) conducted flow visualization tests on a cavity with a heated shroud. When only the shroud was heated (the disks remaining unheated), a similar flow structure to that shown in Figure 2b was observed, except there were multiple radial arms and multiple separation zones. When both the shroud and the disks were heated, the same flow structure as for the heated shroud was observed. In fact, for this to change back to a single radial arm (associated with the heated disk case), the disk temperature was required to be 40°C greater than the shroud temperature.

Farthing et al. (1992a) measured the heat transfer from the disks of a cavity with $a/b = 0.1$ and $G = s/b = 0.138$. They investigated different disk surface temperature distributions and also asymmetrical heating (where one disk is hotter than the other). For symmetrically heated disks, where the level and radial distribution of temperature is the same, the Nusselt numbers are the same on each disk, implying symmetry of the flow in the midaxial plane. For asymmetrically heated disks, the local Nusselt numbers on the cold disk are found to be lower than those on the hot disk. The radial temperature distribution also has a significant effect on the local Nusselt numbers. The radial variation of the Nusselt number follows the disk surface temperature distribution (i.e., for a temperature distribution that increases with radius, Nu also increases with radius and vice versa).

Long and Tucker (1992) have reported on heat transfer measurements from the shroud itself (for $a/b = 0.1$ and $s/b = 0.13$). They noted that the disk surface temperature distribution appears to have little effect on the shroud heat transfer, providing the cavity air temperature is used as a reference temperature to define the Nusselt and Grashof numbers. The shroud heat transfer is then in reasonable agreement with an established correlation for free convection from a horizontal surface. They also noted an enhancement of this heat transfer due to rotationally induced free convection at a Rossby number of approximately 2 and also at Ro > 20.

Tucker (1993) used a 3-D, time-dependent (CFD) code for a numerical investigation of this flow. Predictions were made for laminar flow and also turbulent flow using a mixing-length model. The results were in qualitative agreement with flow visualization results in predicting the features of the flow structure referred to earlier. Disk and shroud Nusselt numbers were in reasonable agreement with measured heat transfer data (considering the relatively large uncertainties in the experimental data at the low flow rates and speeds, and therefore heat fluxes, where most of the comparisons were made). Although encouraging, this approach as a predictive tool is severely bounded due to limitations in CPU time. Typically, 20 hours of Solbourne 5E/905–128 mainframe CPU time are required to advance one second in simulated time.

3. Experimental apparatus

Full design details of the rotating cavity rig can be found in Northrop (1984). The methods used to analyze the experimental data are described by Long (1985, 1987). Modifications relevant to the current tests with the heated shroud are described by Long and Tucker (1992).

A schematic diagram of the experimental rig is shown in Figure 3. Figure 3a shows a side view of the rig. Figure 3b shows an end view illustrating the shroud heater and Figure 3c shows a schematic diagram of the cavity air temperature probe. With the heated shroud, the cavity has an outer radius of $b = 0.4845$m and the disks are separated by an axial distance s (for tests with $G = 0.13$, $s = 0.065$m; for $G = 0.36$, $s = 174$mm). The disks are heated (to a maximum surface temperature of approximately 100°C) by internal electrical heaters; there are five annular 5kW heaters inside each disk. Although this allows the disk surface temperature distribution to be controlled, for the work discussed here this increased with radius (which will be referred to as an increasing temperature distribution). The shroud is heated by an external heater comprising 30 (0.75kW for $G = 0.13$ and 1.25kW for $G = 0.36$) Firebar heater elements. The centerlines of the elements lie parallel to the axis of rotation of the cavity, their active lengths are roughly the width of the outer surface of the shroud and the elements are located in a 270° sector with a 15mm radial clearance from the outer surface of the shroud.

An axial throughflow of air is supplied to the cavity through a hole of radius $a = 0.045$m in the upstream disk. The temperature of this air measured at the cavity inlet (1.65m upstream of the cavity) is T_i. For the tests reported here, T_i was in the range 20–35°C. The air leaves the cavity via an identical hole in the downstream disk. The flow rate is measured by one of a number of devices (depending on the magnitude). At low flow rates $2 \times 10^3 \leq \mathrm{Re}_z \leq 2 \times 10^4$, one of the two Rotameter flow meters on the exit pipe is used. There is some leakage of air into the rig—mainly from the upstream slip ring cooling air. Although the leakage flow is small, it is a significant fraction of the total flow at the lower flow rates. The Rotameters are on the downstream side of the leaks and so give an accurate reading of the flow rate entering the cavity. At higher flow rates ($\mathrm{Re}_z > 2 \times 10^4$), where the leakage is considered not to be as significant, either a 1-inch Annubar, or the pressure drop across the inlet contraction (previously calibrated by Northrop 1984) itself, is used to measure the flow.

The heat transfer measurements are obtained from RdF thermopile flux meters. There are eight of these on each disk and they are located in an instrumentation mat that has a similar thermal conductivity to that of the material used in the

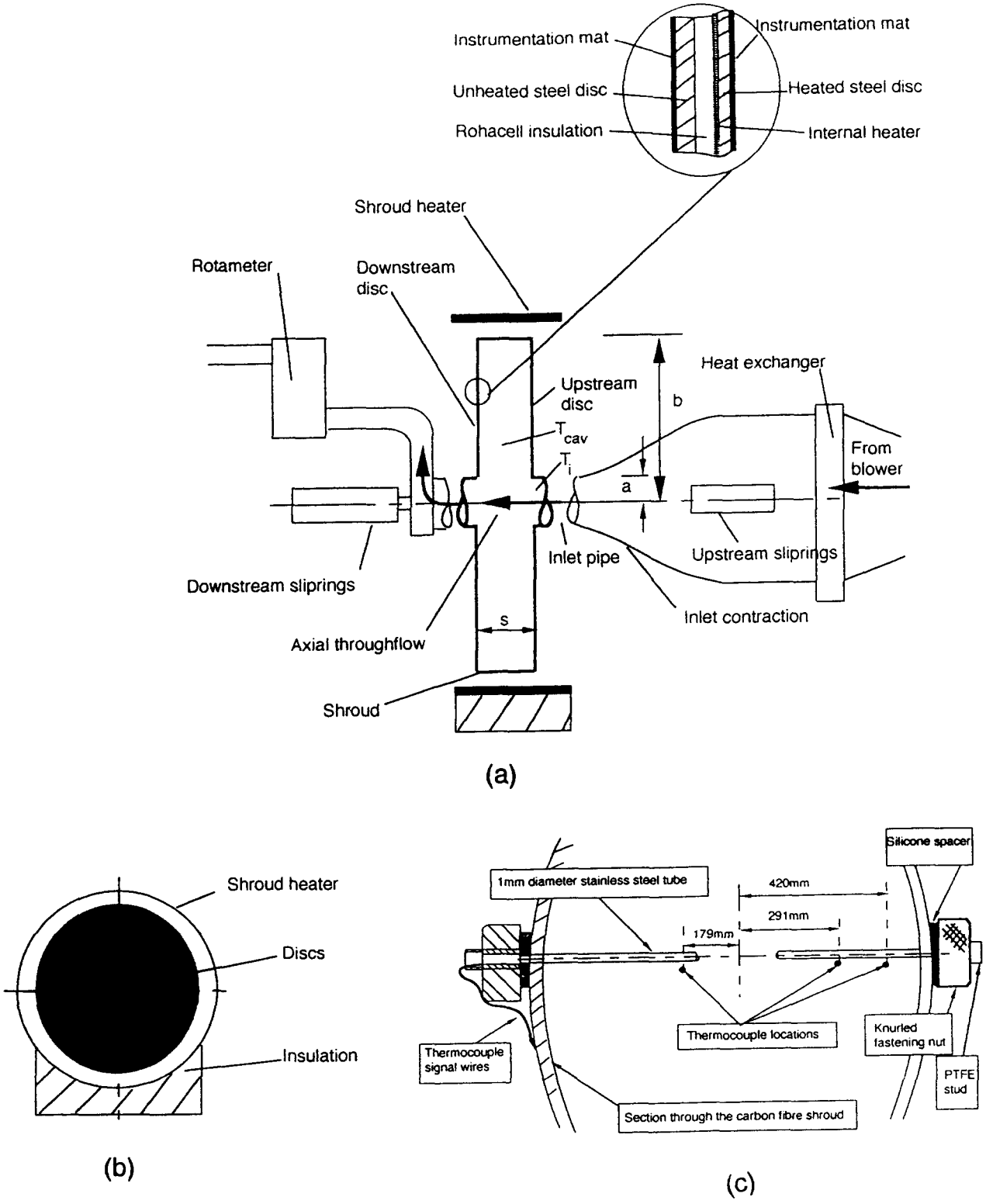

Figure 3 Schematic diagram of the rotating cavity rig: $b = 0.4845$m, $a = 0.045$m; $s = 0.065$m ($G = 0.13$) or 0.174m ($G = 0.36$); (a) side view; (b) end view; (c) cavity air temperature probe

construction of the flux meters. The flux meters were calibrated *in situ* by Long (1991) who used a theoretical model of a thermopile flux meter to predict the heat flux/voltage output characteristic. The calibration was carried out using an impinging flow to cool the disks; heat fluxes obtained from the conduction solution (using measured surface temperatures as boundary conditions to solve the conduction equation for the disks) were used to find values of constants in the theoretical model. The overall accuracy of the flux meters and associated signal-measuring equipment is estimated to be approximately 20W/m^2. For a disk surface-to-air inlet temperature difference of 30°C and at a local radius of $r = 0.3$m, this corresponds to

an uncertainty in Nusselt number of ± 10. The surface temperature of the disks is measured by copper-constantan thermocouples also located in the instrumentation mat; the overall accuracy of the thermocouples is estimated to be ± 0.2°C. There are 13 thermocouples on the outside face of each disk; 23 on the inside face of the upstream disk and 18 on the inside face of the downstream disk.

Details of the unheated shroud can be found in Farthing et al (1992a). For the heated shroud, two different shrouds are used to accommodate the two gap ratios. These are each made from a carbon fiber composite ring of 2.5mm radial thickness, 969 mm internal diameter ($=2b$) and either 127mm ($G = 0.13$) or 240mm ($G = 0.36$) overall axial width. The shroud is located at the outer radius of the disks using a 10mm radial-width layer of silicone foam. Two thermocouples are installed on the shroud: one at $z = s/2$ and one at either $s/3$ for $G = 0.13$ or $z = s/8$ for $G = 0.36$.

The temperature of the air inside the cavity, T_{cav}, is measured using the probe illustrated in Figure 3c. A 1mm diameter stainless steel tube is located at $z = s/2$ and spans the inside of the cavity on a diameter. The tube carries three thermocouples positioned at nondimensional radial coordinates x ($x = r/b$) = 0.369, 0.600 and 0.867. The innermost thermocouple (at $x = 0.369$) is located on one radius of the tube; the other two are located on the diametrically opposing radius. Each thermocouple is constructed from 0.1mm diameter copper-constantan wire. The beads protrude from the surface of the tube by approximately 3mm and are isolated from it using epoxy resin adhesive. These precautions ensure that the local air temperature (not that of the tube) is being measured. Errors associated with conduction along the length of the tube are reduced by using PTFE studs to fix the temperature probe to the shroud. The thermal response time of the thermocouple beads can be estimated using the so-called lumped capacitance equation. Taking a value of heat transfer coefficient for cylinders and wires in cross flow (see Schlicthing 1979), shows that the bead will respond to 87 percent of a step change in temperature in time, $t = C_o\{1/r(\Omega - \omega)\}^{1/2}$ seconds (where $C_o = 0.9\text{m}^{1/2}\text{s}^{1/2}$). For most tests, this is approximately equal to the time taken by the flow inside the cavity to complete one revolution relative to the disks.

4. Surface and air temperature measurements

A typical increasing disk surface temperature distribution is shown in Figure 4, for a test with $G = 0.13$, a rotational Reynolds number of $\text{Re}_\phi = 4 \times 10^5$ and an axial Reynolds number of $\text{Re}_z = 2 \times 10^4$. Although obtained for this particular test condition and from the upstream disk, the radial temperature distribution is similar on the downstream disk and for other values of Re_z and Re_ϕ, and the other gap ratio. The symbols indicate the measured disk and shroud temperatures, and also the air temperature measured inside the cavity T_{cav}. The air inlet temperature T_i is included for reference in Figure 4 and is shown by the dashed line. The radially weighted average and maximum disk temperatures (T_{av} and T_{max}) are approximately 100 and 114°C, respectively. The shroud, which is unheated, has a temperature $T_{sh} = 45$°C and the air inlet temperature T_i is 38°C. There is some radial variation of the air temperature inside the cavity—from 80°C at the innermost location to 72°C at the outermost near the shroud. But of greater significance, the difference between T_{cav} and T_i is 30°C to 40°C.

Temperatures were measured inside the cavity at three radial locations and for $2 \times 10^5 \leq \text{Re}_\phi \leq 2 \times 10^6$; $2 \times 10^3 \leq \text{Re}_z \leq 16 \times 10^4$; $0.03 \leq \beta\Delta T_{av} \leq 0.3$, and with $G = 0.13$ and 0.36. Tests were conducted with heated disks and either an unheated

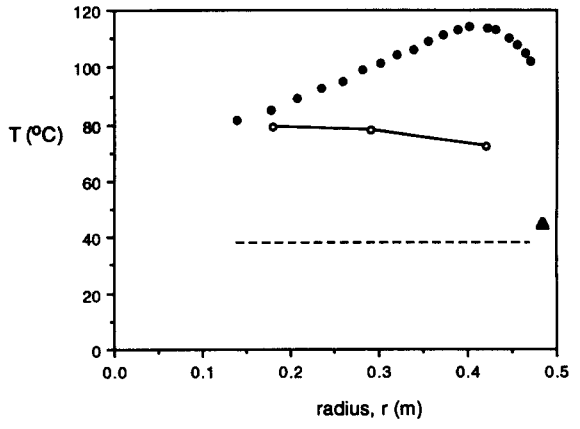

Figure 4 Radial variation of upstream disk surface and cavity air temperatures at $\text{Re}_\phi = 4 \times 10^5$ and $\text{Re}_z = 2 \times 10^4$, and with a disk surface temperature distribution that increases with radius and an unheated shroud; ● = disc surface; --- = inlet air, T_i; ▲ = *shroud surface;* ○ = *cavity air,* T_{cav} *at* $z/s = 0.5$

or heated shroud, and also with a heated shroud and unheated disks. When heated, both disks had the same radial temperature distribution. Details of this work for $G = 0.13$, including the influence of disk surface temperature distribution, can be obtained from Long and Tucker (1992). The following discussion focuses on measurements with the increasing temperature distribution and includes some new results illustrating how the gap ratio influences the cavity air temperature and estimates of the flow entering the cavity itself.

Figure 5 shows the variation of nondimensional cavity air temperature θ_{cav} with axial Reynolds number Re_z. Note that $\theta_{cav} = (T_{av} - T_{cav})/(T_{av} - T_i)$ and the cavity air temperature is taken from the outermost thermocouple bead. For $G = 0.13$, the tests were conducted at a constant value of $\beta\Delta T_{av}$ ($\beta\Delta T_{av} \approx 0.3$), three different axial Reynolds numbers ($\text{Re}_z = 0.2$, 2 and 4×10^4) and three different values of Re_ϕ ($\text{Re}_\phi = 0.2$, 0.4 and 0.8×10^6). For $G = 0.36$, the tests were carried out with $0.03 \leq \beta\Delta T_{av} \leq 0.3$; $\text{Re}_z = 2$, 4 and 16×10^4; and $\text{Re}_\phi = 0.2$, 0.4, 0.8, 1.2 and 2×10^6. Although not included here, as noted by Tucker and Long, the disk surface temperature distribution has far greater influence on θ_{cav} than either Re_ϕ or Re_z. The vertical variation at a given value of Re_z is due to the variation of θ_{cav} with Re_ϕ and/or $\beta\Delta T_{av}$. Increasing either Re_ϕ or $\beta\Delta T_{av}$ tends to increase the air temperature inside the cavity (i.e., θ_{cav} decreases). For the increasing surface temperature distributions tested, θ_{cav} is virtually unaffected by Re_z until $\text{Re}_z > 4 \times 10^4$.

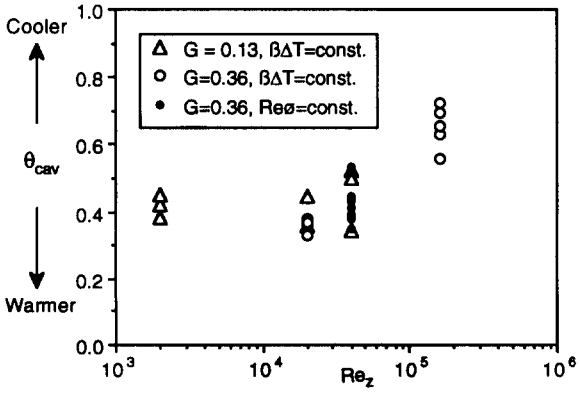

Figure 5 Variation of nondimensional cavity air temperature θ_{cav} with axial Reynolds number Re_z and gap ratio G for T_s *increasing with radius*

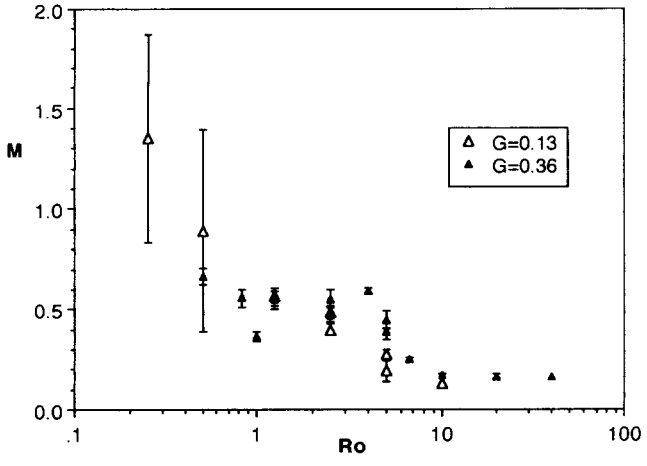

Figure 6 Estimated variation of M, fraction of throughflow to enter the cavity, with Rossby number Ro and gap ratio G

Increasing the axial Reynolds number then increases the value of θ_{cav}—the air becomes cooler inside the cavity. These effects are consistent with the current understanding of the flow inside the cavity. Heating the disks and/or shroud causes the cavity air to be destabilized under the action of rotationally induced forces and air from the throughflow is ingested into the cavity. For a given temperature level, rotation will increase these forces. Consequently, the response of the cavity air temperature to an increase in throughflow rate will depend on the proportion of air ingested to that of the throughflow.

This point is illustrated in Figure 6, which shows the estimated variation of the fraction of the axial throughflow, which enters the cavity M, with Rossby number Ro. The values of M are obtained from a heat balance using measured values of average disk heat transfer and cavity air temperature. Assuming complete and even mixing inside the cavity, equal upstream and downstream disk average temperatures and heat fluxes and no shroud heat transfer, it is easily shown that

$$M = 4(b/a)\mathrm{Nu}_{av}/\{(1 - \theta_{cav})\mathrm{Re}_z\mathrm{Pr}\} \quad (1)$$

where Nu_{av} is taken as the average of the radially weighted average Nusselt numbers from the two disks. Also shown are bounds to the estimate of M corresponding to uncertainty in the average Nusselt number of ± 10.

Figure 6 shows that a significant fraction of the throughflow can enter the cavity and that the Rossby number is a useful parameter in estimating this quantity. It also illustrates the competing interaction between the axial momentum of the throughflow air and thermal entrainment due to rotation. The tests for $\mathrm{Ro} < 0.5$ with $G = 0.13$ were carried out with $\mathrm{Re}_z = 2 \times 10^3$, where the measured heat fluxes are relatively low and, as indicated, the error bounds are large. The measured value of $M > 1$ at $\mathrm{Ro} = 0.2$ is physically impossible and is attributed to experimental uncertainty and/or the assumptions made concerning equal and even mixing. (Equation 1 provides an upper bound to M if the flow is not evenly mixed.) Nonetheless, it appears that for $\mathrm{Ro} < 1$, at least 50 percent of the throughflow enters the cavity; for $\mathrm{Ro} > 10$, this reduces to approximately 10 percent. The variation between these two extrema is relatively continuous and shows some dependence on the gap ratio. The data for $G = 0.36$ show a sudden jump around $\mathrm{Ro} = 5$, possibly due to the action of vortex breakdown; the data for $G = 0.13$ show a smoother variation. Apart from this difference around $\mathrm{Ro} = 5$, there does not appear to be a significant (i.e., in proportion to the difference in gap ratio) difference in M for the two gap ratios tested.

5. Heat transfer: results and discussion

The Nusselt numbers discussed in this section were obtained from the flux meters and heat transfer tests were carried out with $G = 0.13$ and $G = 0.36$. The discussion here will focus on the results for a surface temperature that increases with radius (see Figure 4) with both disks having the same radial distribution of temperature. Most tests were conducted with the same surface-to-air temperature difference ($\beta\Delta T_{max} \approx 0.27$). However, some tests were also carried out to investigate the effect on the heat transfer of varying the buoyancy parameter. In these tests, $0.12 \leq \beta\Delta T_{max} \leq 0.36$. Unless stated otherwise, the shroud was heated and the shroud temperature was equal to the maximum surface temperature of the disks. The tests covered the range of axial and rotational Reynolds numbers: $2 \times 10^4 \leq \mathrm{Re}_z \leq 16 \times 10^4$ and $2 \times 10^5 \leq \mathrm{Re}_\phi \leq 5 \times 10^6$. As shown by Farthing et al. (1992a), the temperature distribution is known to significantly affect the local Nusselt numbers, but to date it has not been possible to characterize this effect. Consequently, all heat transfer measurements were obtained under steady-state conditions because there can be significant changes in the disk's surface temperature distribution during transient (heating or cooling) tests.

The brief description given in Section 2 and Figure 2 illustrates that the heated flow structure is nonaxisymmetric, which raises the question: Is the resulting heat transfer distribution also nonaxisymmetric? A series of tests were

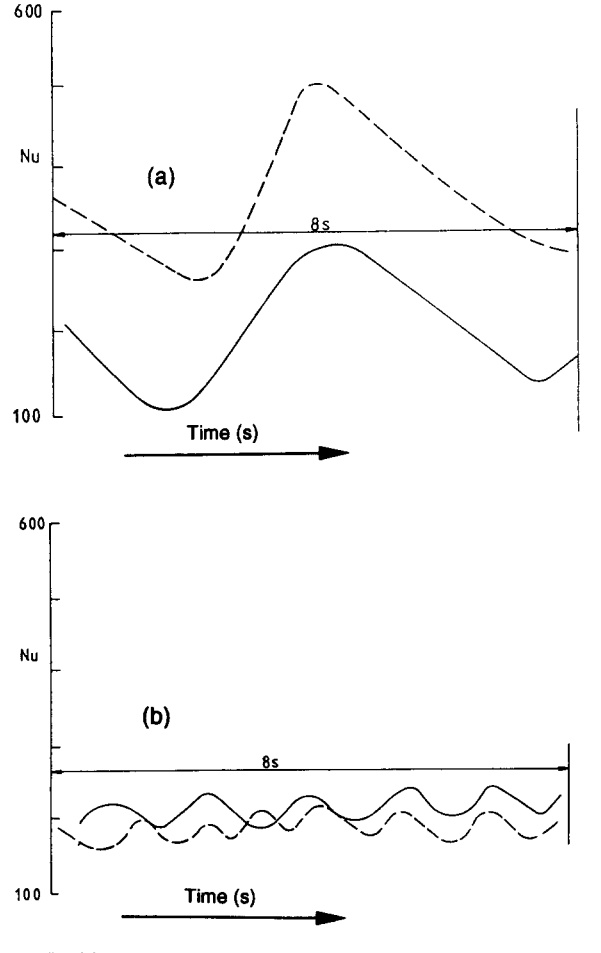

Figure 7 Measured variations of local Nusselt number, $\mathrm{Nu} = qr/(T_s - T_i)k$, with time on the downstream disk with $G = 0.36$ and $\mathrm{Re}_z = 16 \times 10^4$: (a) $\mathrm{Re}_\phi = 2 \times 10^5$; (b) $\mathrm{Re}_\phi = 8 \times 10^5$; ——— = flux meter No. 5 at $x = 0.72$; --- = flux meter No. 7 at $x = 0.82$

conducted in which the output from a single flux meter was measured rapidly (approximately 13Hz). The results, shown as a variation in the local Nusselt number (defined using the radius as the characteristic length), $Nu = qr/(T_s - T_i)k$, against time for flux meters No. 5 (at $x = 0.72$) and No. 7 (at $x = 0.82$) with $G = 0.36$ and at $Re_\phi = 2 \times 10^5$ and $Re_z = 16 \times 10^4$, are illustrated in Figure 7(a), and for $Re_\phi = 8 \times 10^5$ and $Re_z = 16 \times 10^4$, in Figure 7b. Both flux meters show a similar variation of Nusselt number with time. In Figure 7a, the period is approximately 5.5 seconds, which (assuming that this variation is repeated once for each revolution of the flow relative to the disk) implies that the flow is rotating at 91 percent of the disk speed. The difference between the maximum and minimum Nusselt numbers is about 250. However, the correspondence between the curves and the flow structure is not yet established (i.e., where in relation to the features of the flow field do the maximum and minimum Nusselt numbers occur?).

The response time (to 62 percent of a step change in heat flux) for these flux meters, according to the manufacturer's data, is 0.4 seconds, which is sufficient to give an accurate record for the variations shown in Figure 7a. For the results shown in Figure 7b (at a higher rotational speed and flow rate, $Re_\phi = 8 \times 10^5$ and $Re_z = 16 \times 10^4$), the period between peaks in Nu is approximately 1.5s. The actual variation of Nusselt number is likely to exceed that recorded due to the limitation of the response time.

Subsequent heat transfer results are presented as a time average of 100 instantaneous values recorded during each test. To avoid errors caused by numerical smoothing of the data, the first and last ten values are not used in evaluating this average. The signals from each flux meter are recorded using an integration time of 20ms (at $Re_\phi = 2 \times 10^5$, this corresponds to 1/25th of a revolution), which is small relative to the period between successive measurements from the same flux meter (approximately 10s). It is also unlikely that a measurement will be repeated at exactly the same time relative to the flow. Consequently, the measurements of heat transfer presented here should be considered as averages of these snapshot measurements. Due to the relatively large number of measurements, it is likely that the presented averages will represent a true time average.

5.1. The effect of gap ratio, axial and rotational Reynolds numbers

The effect on the disk heat transfer of the axial and rotational Reynolds numbers is addressed by looking at results from some individual flux meters. Since all these tests were carried out with similar values of local surface-to-air inlet temperature differences, such an approach eliminates the need, at this stage, to account for the buoyancy parameter. Similarly, the discussion need not concern the choice of characteristic length scale, radius is used and $Nu = qr/(T_s - T_i)k$. Heat transfer measurements, for $G = 0.13$ with an unheated shroud, from flux meters 1, 4 and 7 (located at $x = 0.417$, 0.753 and 0.929) are shown in Figure 8. The horizontal axis is the Rossby number, Ro, and the Nusselt number is normalized with respect to the axial Reynolds number Re_z. These scales are chosen to allow the different effects of speed and flow rate to be assessed for the range of experimental conditions. For $G = 0.13$, the results from the upstream and downstream disks are similar, which as noted by Farthing et al (1992a), indicates symmetry of the flow about the mid axial plane. The most immediate difference is in the shape of the results obtained from the innermost flux meter compared with those further into the cavity. The evidence shown here suggests that Nu/Re_z varies as Ro^{-n}. The magnitude of n actually increases with increasing radius (at

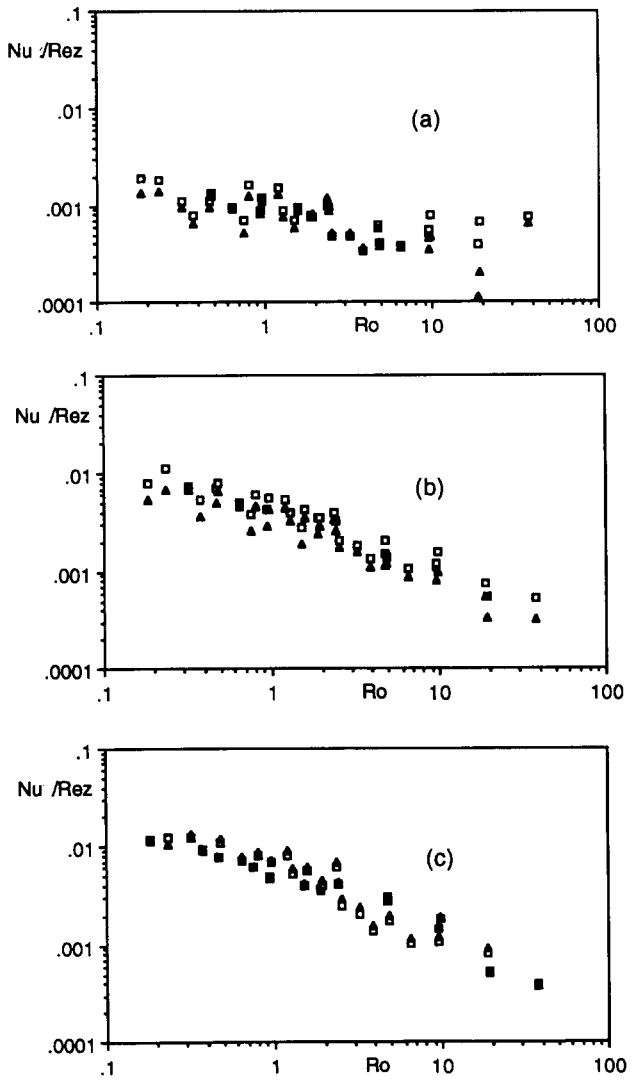

Figure 8 Variation of Nu/Re_z ($Nu = qr/[T_s - T_i]k$) from individual flux meters with Rossby number, Ro, for $G = 0.13$; (a) flux meter No. 1 ($x = 0.417$); (b) flux meter No. 4 ($x = 0.753$); (c) flux meter No. 7 ($x = 0.929$); □ = upstream disk; ▲ = downstream disk

$x = 0.753$, $n \approx 2/3$ and at $x = 0.929$, $n \approx 1$). This implies that the axial Reynolds number has increasingly less effect on the heat transfer at the larger radii, where the main influence is the rotational Reynolds number and, as will be shown later, the increasing influence of buoyancy forces. For flux meter No. 1 (and to a lesser extent the other flux meters), there is a distinct jump located at $Ro \approx 2.5$ that could be attributable to vortex breakdown affecting the heat transfer. For the innermost flux meter, $n \approx 1/3$; the axial Reynolds number has the major influence on the heat transfer, which is not surprising considering the radial location. For small values of the Rossby number (i.e., $Ro < 0.8$), there is a leveling ($Nu/Re_z \approx$ constant) in the data implying that the Nusselt number is not affected by the rotational Reynolds number. Since this occurs at large values of Re_ϕ, and/or small values of Re_z, the result may seem paradoxical. However, as shown in Figure 6 (where for $Ro < 1$,50 percent of the throughflow is estimated to enter the cavity), it is considered to be caused by a saturation effect. All, or the maximum, of the available throughflow has entered the cavity—a reduction in the Rossby number through increasing Re_ϕ or decreasing Re_z will not change the amount ingested, so the heat transfer does not increase.

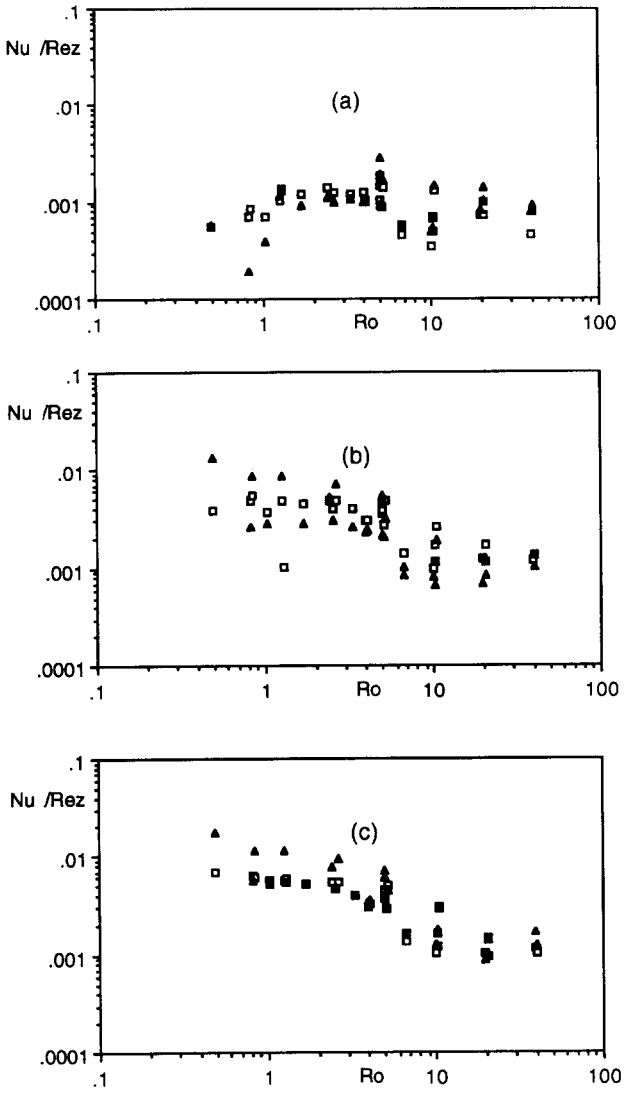

Figure 9 Variation of Nu/Re_z ($Nu = qr/[T_s - T_i]k$) from individual flux meters with Rossby number, Ro, for $G = 0.36$; (a) flux meter No. 1 ($x = 0.36$); (b) flux meter No. 4 ($x = 0.66$); (c) flux meter No. 7 ($x = 0.82$); □ = upstream disk; ▲ = downstream disk

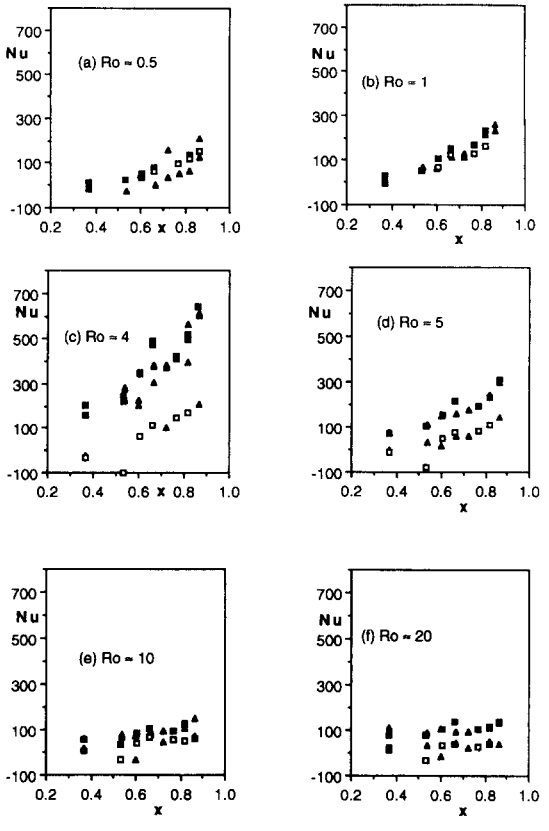

Figure 10 Radial variation of local Nusselt numbers ($Nu = qr/[T_s - T_i]k$) for different values of Ro and gap ratios

	$G = 0.13$	$G = 0.36$
Upstream disk	□	■
Downstream disk	△	▲

Corresponding results from the larger gap ratio ($G = 0.36$) cavity are shown in Figure 9. These appear to have quite a different characteristic shape to the small gap ratio cavity. The region where $Nu/Re_z \approx Ro^{-n} (n \neq 0)$ is still present but is now seen to extend over a limited range of the Rossby number ($2.5 \leq Ro \leq 10$). For larger values of Ro in the wider cavity, where the momentum of the axial jet is sufficiently large, Re_z appears to be the major controlling parameter and leads to a significant increase in heat transfer over the narrower cavity. For smaller values of Ro, the saturation effect referred to earlier causes a leveling, or even a reduction, in the heat transfer. There are also clear differences between upstream and downstream disk results—particularly for flux meters 1 and 4—and are attributed to the increased circulation in the wide gap ratio cavity. For flux meter No. 1, there is scatter in the data around $Ro \approx 5$ which as noted earlier, for the cavity with $G = 0.13$ at $Ro \approx 2.5$, is possibly attributable to vortex breakdown.

The radial variations of Nusselt number for the two cavities are compared in Figure 10. Increasing the gap ratio has a variety of influence on the heat transfer. For the region $4 \leq Ro \leq 5$, there is a marked increase in heat transfer. For $Ro > 5$, there is less of an increase and, for $Ro < 4$, the heat transfer does not appear to be significantly affected by gap ratio.

Referring back to Figure 5 shows that changing the gap ratio from $G = 0.13$ to $G = 0.36$ does not significantly change the cavity air temperature. Therefore, any differences must be due to a difference in flow behavior. At larger values of the Rossby number (say $Ro > 5$), the flow is considered to be controlled by the central throughflow—a relatively large gap ratio will allow this to more easily influence the flow and heat transfer inside the cavity. At small values of the Rossby number it is considered that forces induced by rotation control the flow and these are unlikely to be affected by the gap ratio. The substantial increase in disk heat transfer with an increase in gap ratio for the region $4 \leq Ro \leq 5$ appears to occur as a result of vortex breakdown in the wider gap ratio cavity. There is considerable evidence showing that various forms of vortex breakdown do occur (Farthing et al. 1992b) and, indeed, Long and Tucker (1992) noted an effect on the shroud heat transfer in the range $2 \leq Ro \leq 4$.

The observations discussed in the previous three figures illustrate the complex nature of this flow. Yet, despite attempts, it has not been possible to produce a universal correlation that takes into account the effects of all parameters investigated (gap ratio, and axial and rotational Reynolds numbers).

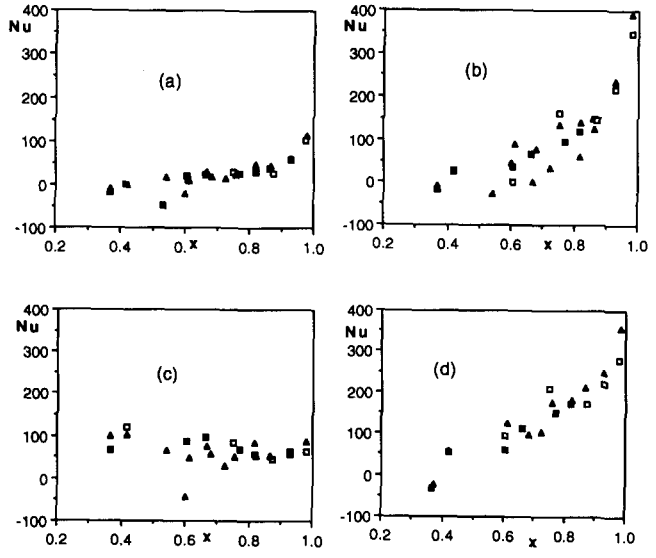

Figure 11 Radial variation of local Nusselt numbers ($Nu = qr/[T_s - T_i]k$) with and without a heated shroud: (a) $Re_z = 2 \times 10^4$, $Re_\phi = 2 \times 10^5$; (*b*) $Re_z = 2 \times 10^4$, $Re_\phi = 2 \times 10^6$; (c) $Re_z = 16 \times 10^4$, $Re_\phi = 2 \times 10^5$; (d) $Re_z = 16 \times 10^4$, $Re_\phi = 2 \times 10^6$

	Unheated shroud	Heated shroud
Upstream disk	□	■
Downsteam disk	△	▲

5.2. The effect of shroud temperature

Figure 11 shows the radial variation of local Nusselt numbers (measured from both disks) for $G = 0.13$ and for tests at $Re_z = 2 \times 10^4$, $Re_\phi = 2 \times 10^5$, $Re_z = 2 \times 10^4$, $Re_\phi = 2 \times 10^6$; $Re_z = 16 \times 10^4$, $Re_\phi = 2 \times 10^5$ and $Re_z = 16 \times 10^4$, $Re_\phi = 2 \times 10^6$. In one set of tests, the shroud was heated to approximately the maximum disk temperature (100°C). In the other set of tests, the shroud was unheated. (As shown in Figure 4, the surface temperature was usually in the range 30–40°C.) Note, although the physical location of the flux meters remained the same for these two sets of tests, there is a difference in their nondimensional location due to differences in shroud design.

For most of the experimental conditions shown here (which represent the extreme of the range of Re_z and Re_ϕ tested with the heated shroud, but a similar result applies at the intermediate values of Re_z and Re_ϕ), heating the shroud does not appear to significantly affect the disk heat transfer. The exception occurs when the Rossby number is low (for example, the results at $Re_z = 2 \times 10^4$ and $Re_\phi = 2 \times 10^6$), where there is a small reduction in disk heat transfer when the shroud is heated. This is expected, since at low values of Ro most of the available throughflow enters the cavity and the cavity air temperature is appreciably increased when the shroud is also heated. The effect is a reduction in the disk surface heat flux and, because the Nusselt number is defined using the inlet temperature to the cavity, a reduction in Nu. Although not shown here, other tests were carried out with a heated shroud having an intermediate temperature between the disks and inlet air, and also with a shroud heated above the maximum disk temperature. In both cases, similar effects were noted: there is a small difference at lowest values of Re_z and highest values of Re_ϕ, elsewhere there is no significant difference.

5.3. The effect of buoyancy parameter $\beta\Delta T$

In the previously discussed results, the buoyancy parameter $\beta\Delta T_{max}$ remained sensibly constant ($\beta\Delta T_{max} \approx 0.27$). A limited number of tests were also carried out at constant axial and rotational Reynolds numbers, varying $\beta\Delta T_{max}$ in the range $0.12 \leq \beta\Delta T_{max} \leq 0.36$. It is recognized that the radial surface temperature distribution on the disks has a major influence on the local Nusselt numbers and so care was taken during the course of these tests to ensure similar temperature distributions.

The radial variation of measured Nusselt numbers on the upstream disk for $G = 0.13$, $Re_z = 8 \times 10^4$, $Re_\phi = 2 \times 10^6$ (and with a heated shroud) is shown in Figure 12a. Five different

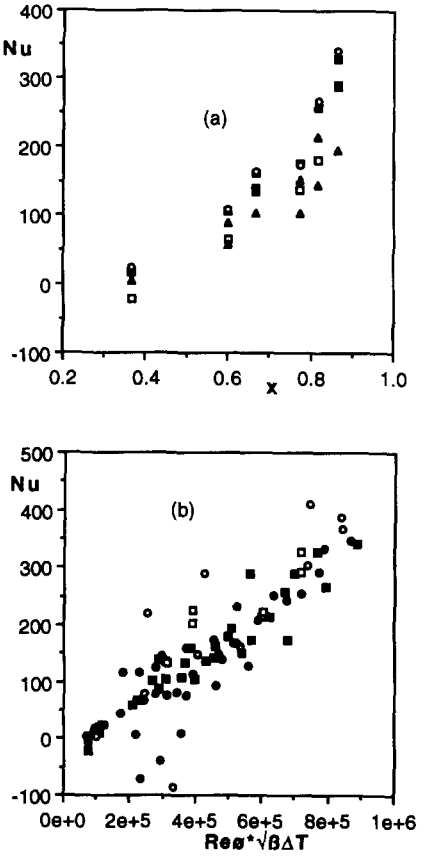

Figure 12 Variation of local Nusselt numbers ($Nu = qr/[T_s - T_i]k$) with buoyancy parameter for $G = 0.13$, $Re_z = 8 \times 10^4$ and $Re_\phi = 2 \times 10^6$

(a) Radial variation of upstream disk results

symbol	$\beta\Delta T_{max}$
△	0.120
□	0.147
▲	0.225
■	0.270
○	0.362

(b) Variation with parameter $Re_\phi^* \sqrt{\beta\Delta T}$

	constant $\beta\Delta T_{max}$	variable $\beta\Delta T_{max}$
Downstream disk	○	●
Upstream disk	□	■

values of $\beta\Delta T_{max}$ were used in these tests and the plot clearly shows that the Nusselt numbers are influenced by the buoyancy parameter. For the conditions here, Ro $\approx$ 2 rotation, in particular rotationally induced buoyancy, is expected to affect the heat transfer. In general, at any radius the lowest values of the Nusselt number correspond to the lowest value of $\beta\Delta T_{max}$ and vice versa. The variation also appears to become larger toward the outer radius, where the buoyancy forces are larger.

An attempt to correlate these data is shown in Figure 12b. Although there is a fair degree of scatter, the measured values of Nu do have reasonable correlation with the product of the local rotational Reynolds number and the square root of the buoyancy parameter, $Re_\phi^* \sqrt{\beta\Delta T}$. There is some difference between these results and those obtained from a series of tests where $\beta\Delta T_{max}$ is held constant and Re_z and Re_ϕ are varied. The difference is considered to be due to a difference in disk surface temperature distributions. The tests where $\beta\Delta T_{max}$ is varied result in a much flatter temperature distribution (because the rig is operating at a high speed for much longer and heat is conducted from the bearings to the inner radii of the disks) and, consequently, a reduced heat transfer level. However, many different correlating parameters were tried and this was found to give the best fit to the data.

6. Conclusions

Tests were carried out on a single rotating cavity comprised of two disks of radius $b = 0.4845$m bounded at the circumference by a carbon fiber shroud. Experiments were conducted for the range of parameters $0.03 \leq \beta\Delta T \leq 0.3$, $2 \times 10^3 \leq Re_z \leq 16 \times 10^4$ and $2 \times 10^5 \leq Re_\phi \leq 5 \times 10^6$; for cavity gap ratios $G = 0.13$ and 0.36; and a constant value of inlet radius ratio of $a/b = 0.1$. Different thermal conditions were investigated: heated disks and shroud or heated disks and an unheated shroud. Measurements were made of the air temperature inside the cavity by three thermocouple probes located on a diameter halfway between the two disks (at $z = s/2$). The heat transfer from the disks was measured using thermopile flux meters—eight on the surface of each disk.

The gap ratio appears to have little significant effect on the nondimensional cavity air temperature. The measurements of cavity air temperature and cavity heat transfer were used to estimate the fraction of the central throughflow entering the cavity. This is only slightly dependent on the gap ratio. For Ro < 1, approximately 50 percent is found to enter the cavity and for Ro > 10 this decreases to around 10 percent.

The heat transfer tests were carried out with the same surface temperature distribution, which increased with radius, on both disks. Two mechanisms appear to operate in influencing the heat transfer in a rotating cavity with axial throughflow. Firstly, heating of the air inside the cavity destabilizes it and convection occurs under the action of rotationally induced buoyancy forces. Secondly, the central throughflow encourages mixing with the cavity air, which can either affect the heat transfer directly (as, for example, at the inner radii of the disks) or indirectly through the action of vortex breakdown. It is apparent that there are complex interactions between the flow rate, buoyancy parameter, rotational speed and the geometry. These all play a role in affecting the disk heat transfer. It is, however, a complex phenomenon that involves both free- and forced-convection effects. For the smaller gap ratio cavity, rotational effects become increasingly important toward the outer radius across a wide range of Rossby numbers. For the wider gap ratio cavity, this is restricted to a narrower range of Ro. In the region $4 \leq Ro \leq 5$, the gap ratio plays a crucial role in affecting the disk heat transfer. At smaller values of Ro, where a significant fraction of the throughflow enters the cavity, the disk heat transfer rate does not appear to be affected by gap ratio. At larger values, increasing the gap ratio also increases the heat transfer.

Heating the shroud does not appear to significantly affect the heat transfer from the disks (although there is a small reduction at small values of Ro).

The dependence of the Nusselt numbers on the buoyancy parameter has been verified but the precise dependence has not yet been established. This should certainly be addressed in future work. The work has also, almost exclusively, considered symmetric heating (where both disks have the same temperature distribution and maximum temperature). In a real engine, this is not the case and now that the basic flow is understood, future work should be directed toward simulating conditions that occur inside an engine—both in terms of more realistic thermodynamic parameters and the geometry.

Acknowledgments

The author wishes to thank Dr. Paul Tucker and Mr. Güven Kais for their help in obtaining most of the experimental data discussed here under what were at times difficult circumstances. I am also grateful for the past help of Prof. Mike Owen, a former colleague and now Professor of Mechanical Engineering at Bath University. Finally, my appreciation must be extended to the organizations that have funded this research, notably The Science and Engineering Research Council and Rolls-Royce plc.

References

Farthing, P. R. 1988. The effect of geometry on flow and heat transfer in a rotating cavity. Ph.D. Thesis, School of Engineering and Applied Sciences, University of Sussex, UK

Farthing, P. R., Long, C. A., Owen, J. M. and Pincombe, J. R. 1992a. Rotating cavity with axial throughflow of cooling air: heat transfer. *ASME Journal of Turbomachinery*, **114**, 229–236

Farthing, P. R., Long, C. A., Owen, J. M. and Pincombe, J. R. 1992b. Rotating cavity with axial throughflow of cooling air: flow structure. *ASME Journal of Turbomachinery*, **114**, 237–246

Long, C. A. 1985. Transient analysis of experimental data from the Mark II rotating cavity rig. *Report no. 85/TFMRC/76*, School of Engineering, University of Sussex, UK

Long, C. A. 1987. Heat transfer in a rotating cylindrical cavity with an axial throughflow of cooling air. Part 1: experimental results for $G = 0.136$ and $X_1 = 0.1$. *Report no. 87/TFMRC/106*, School of Engineering, University of Sussex, UK

Long, C. A. 1991. A calibration technique for thermopile heat-flux gauges. *Proceedings of Sensor 91 Conference, IV* (Paper no. B12.2), Nuremberg, Germany, 247–262

Long, C. A. and Tucker, P. G. 1992. Shroud heat transfer measurements from a rotating cavity with an axial throughflow of air. *37th ASME International Gas Turbine Conference* (Paper no. 92-GT-69), Cologne

Northrop, A. N. 1984. Heat transfer in a cylindrical rotating cavity. Ph.D. Thesis, School of Engineering and Applied Sciences, University of Sussex, UK

Schlichting, H. 1979. *Boundary-Layer Theory*. 7th Ed., McGraw-Hill, New York

Tucker, P. G. 1993. Numerical and experimental investigation of flow structure and heat transfer in a rotating cavity with an axial throughflow of cooling air. Ph.D. Thesis, School of Engineering, University of Sussex, UK